

## Search for collective behavior in very small and in large systems

SANDRA S. PADULA for the CMS COLLABORATION  
*SPRACE and IFT, UNESP - São Paulo, SP, Brazil*

received 23 July 2024

**Summary.** — Signs of collectivity were initially seen in AuAu collisions at RHIC through measurements of two-particle long-range correlations in (pseudorapidity)  $\Delta\eta$ , within small (azimuthal)  $\Delta\phi$  angles. In 2010 a similar ridge-like behavior was observed in high multiplicity pp collisions at 7 TeV at the LHC by CMS, extended afterwards also to pPb and PbPb collisions. In addition, several orders of anisotropic flow Fourier harmonics were measured later, showing a collective behavior compatible with hydrodynamic expectations. This posed the question about the threshold on system size and conditions for collectivity to arise. Signs of possible collectivity were then searched for in  $e^+e^-$  and ep at LEP, in  $\gamma p$  and  $\gamma A$  at the LHC, but usually limited to lower multiplicity ranges ( $< 40$  particles per event), where collectivity was not expected, with negative results. However, more recent investigations with higher multiplicity data collected with the ALEPH experiment at LEP II energies seem to indicate a different picture. This talk shows recent results from the CMS Collaboration for two extreme sizes of colliding systems. On the lowest side, the results focus on the search for a ridge-like behavior in high multiplicity pp collisions at 13 TeV inside a single jet, originated from a highly energetic parton. On the other extreme, PbPb collisions at  $\sqrt{s_{NN}} = 5.02$  TeV are employed to probe deeper into the quark-gluon plasma formed in such collisions, by measuring the speed of sound and the effective temperature in this medium.

### 1. – Search for collectivity in the smallest possible system sizes

Quantum Chromodynamics is the theory that describes the strong interaction among quarks and gluons; in the low-energy limit, these partons are confined inside the hadrons, however, in the very high energy regime, such as those in nucleus-nucleus (AA) collisions at RHIC and LHC, a hot and dense medium of nearly free partons (quark-gluon plasma – QGP) is formed [1-4]. The extremely high densities produced in such collisions result in strong partonic rescatterings that propel the system toward a nearly ideal hydrodynamic limit. This leads to an extended structure (“ridge”) in pseudorapidity  $\Delta\eta$  and in small (azimuthal)  $\Delta\phi$  angles in dihadron correlations, discovered at the BNL RHIC in AuAu [5] and later also observed in PbPb [6] and pPb [7] collisions at the CERN LHC.

Surprisingly, this ridge-like structure was also observed in 2010 in high multiplicity proton-proton (pp) collisions [8] at  $\sqrt{s_{NN}} = 7$  TeV at the LHC by CMS. This unexpected result motivated later searches for the lowest size limit and conditions of colliding systems under which equivalent collective phenomena could be observed. Therefore, similar

correlation studies in  $e^+e^-$  [9,10], ep [11,12],  $\gamma p$  [13] and  $\gamma A$  [14] systems were performed, in which no near-side ridge could be revealed, although only relatively low-multiplicity events (less than 30-40 charged particles) were used in the analyses. More recently, additional measurements of two-particle angular correlations in  $e^+e^-$  collisions [36] were performed with 183-209 GeV data from ALEPH Collaboration at LEP II, allowing to reach higher multiplicities. Analyzing these data with respect to the thrust axis of these collisions, a long-range near-side excess in the correlation function emerged. Besides, the two-particle correlation functions in  $e^+e^-$  collisions were decomposed for the first time using a Fourier series. The resulting Fourier coefficients  $v_n$  from LEP-II provided a comparison to the archived Monte Carlo (MC) [36], especially in high multiplicity events where particle counts exceeded 50; the magnitudes of  $v_2$  and  $v_3$  in data were larger than those in the MC reference.

Moreover, in ref. [15], it is postulated that QCD collective effects could emerge from an initial system as small as a very energetic scattered parton as it traverses through vacuum, and gives rise to a collimated spray of hadrons (jet) as it fragments and hadronizes. For probing such a possibility in a system as small as a jet, but that leads to a very high multiplicity of particles, CMS investigated  $138 \text{ fb}^{-1}$  of high-pileup 13 TeV pp collisions [16]. Jets were selected in this sample by their charged particle multiplicity, after applying the PUPPI pileup subtraction [17]. The data were collected using an online trigger searching for events containing anti- $k_T$  jets [18,19] with distance parameter  $R = 0.8$  and having a transverse momentum ( $p_T$ ) above 500 GeV. In the offline analysis, jets were required to have a  $p_T > 550$  GeV. Additionally, each jet contribution was weighted by the inverse of the trigger efficiency at that jet's  $p_T$ . Jets were also required to have pseudorapidity  $|\eta| < 1.6$  in the laboratory reference frame. Two MC event generators were used in this analysis: PYTHIA8.306 [20] with the CP5 tune [21] and SHERPA2.2 [22]. Jet energy corrections were derived from MC simulations, with the aim that the average measured energy of jets becomes identical to that of particle-level jets.

This analysis deals with the charged constituents of jets, which are required to be within  $|\eta| < 2.4$  and  $p_T > 50.3$  GeV in the laboratory reference frame. The two-particle correlation analysis is similar to that employed in ref. [7], however the momentum vectors of all charged constituents of a jet are defined in the ‘‘jet basis’’, as illustrated in fig. 1 of ref. [15]. A unique jet reference coordinate basis is defined for every jet such that the z-axis is aligned with the direction of the jet momentum. Next, momentum vectors of charged constituents redefined in this new basis are aligned with the direction of the jet momentum:  $\vec{p}^* = (j_T, \eta^*, \phi^*)$ , where  $j_T$  is the particle  $p_T$  with respect to the jet axis. The symbols  $\eta^*$  and  $\phi^*$  are the pseudorapidity and azimuthal angle coordinates with respect to the jet axis. Therefore,  $\eta^* = 0$  and  $\infty$  correspond to vectors that are perpendicular and parallel to the jet axis, as illustrated in fig. 1 of ref. [15]. In this system,  $\eta^* = 0.86$  is the approximate boundary of the anti- $k_T$  jet. The azimuthal coordinates of tracks that are approximately parallel to the direction of the jet axis ( $\eta^* > 5$ ) are sensitive to small changes in the jet axis direction caused by resolution effects. Therefore, such tracks are excluded in the subsequent analysis. Reconstructed particles in the event that are not clustered into the jet of interest are not considered.

For each jet with  $p_T > 550$  GeV, the two-dimensional (2D) angular correlation function is calculated using charged constituents from the jet as follows:

$$(1) \quad \frac{1}{N_{\text{ch}}^{\text{trg}}} \frac{d^2 N^{\text{pair}}}{d\Delta\eta^* d\Delta\phi^*} = B(0,0) \frac{S(\Delta\eta^*, \Delta\phi^*)}{B(\Delta\eta^*, \Delta\phi^*)},$$

where  $\Delta\eta^*$  and  $\Delta\phi^*$  are the relative pair separation in pseudorapidity and azimuthal angle in the jet basis. The functions  $S(\Delta\eta^*, \Delta\phi^*) = \frac{1}{N_{\text{ch}}^{\text{trg}}} \frac{d^2 N^{\text{sig}}}{d\Delta\eta^* d\Delta\phi^*}$  and  $B(\Delta\eta^*, \Delta\phi^*) = \frac{1}{N_{\text{ch}}^{\text{trg}}} \frac{d^2 N^{\text{combin}}}{d\Delta\eta^* d\Delta\phi^*}$ , represent the signal and combinatorial distributions, respectively;  $N^{\text{sig}}$  and  $N^{\text{combin}}$  are the numbers of signal and combinatorial pairs, respectively, and  $N_{\text{ch}}^{\text{trg}}$  is the number of particles within a specific  $j_T$  range used to calculate the correlation functions. The measurement is performed as a function of  $f N_{\text{ch}}^j$ , the  $j_T$ -inclusive in-jet charged multiplicity after correcting for detector effects. Equation (1) is constructed for jets in various classes of  $N_{\text{ch}}^j$ , such that the jets used to populate the  $S(\Delta\eta^*, \Delta\phi^*)$  and  $B(\Delta\eta^*, \Delta\phi^*)$  distributions fall within a specific range of  $N_{\text{ch}}^j$ . The  $S(\Delta\eta^*, \Delta\phi^*)$  distribution is calculated with charged particles paired from the constituents of each unique jet individually, and then averaged over all jets. The combinatorial distribution serves as both a reference and a correction to the pair acceptance due to the limited  $\eta^*$  range. To construct the  $B(\Delta\eta^*, \Delta\phi^*)$  distribution, a two-dimensional (2D) single-particle  $\eta^* - \phi^*$  distribution for charged constituents of all jets within the  $N_{\text{ch}}^j$  range chosen for the signal distribution is first derived. Pairs of  $(\eta^*, \phi^*)$  points from this distribution are then randomly selected to construct  $B(\Delta\eta^*, \Delta\phi^*)$ . Correlations present in the signal distribution that are related to single-particle distributions or detector effects can be canceled by the  $B(0, 0)/B(\Delta\eta^*, \Delta\phi^*)$  term in eq. (1). The short-range correlations are excluded by requiring  $|\Delta\eta^*| > 2$ . The resulting 2D distribution can be further studied by integrating over  $|\eta^*| > 2$  and decomposing into a 1D Fourier series:

$$(2) \quad \frac{1}{N_{\text{ch}}^{\text{trg}}} \frac{dN^{\text{pair}}}{\Delta\phi^*} \propto 1 + 2 \sum_{n=1}^{\infty} V_{n\Delta}^* \cos(n\Delta\phi^*).$$

The strength of the Fourier components in this decomposition could be an indicator of the existence of collective effects. The main observable of interest is the single-particle elliptic anisotropy coefficient,  $v_2^*$ , related to the two-particle Fourier coefficient by (assuming factorization)  $v_2^* = \sqrt{V_{2\Delta}^*}$ . Results are presented as a function of  $\langle N_{\text{ch}}^j \rangle$ , the average of  $N_{\text{ch}}^j$ . The total sample contained more than 100 million events, from which 2,500 were selected on the top  $N_{\text{ch}}^j$  multiplicities.

The measurements for the ridge-like structure were performed in several multiplicity ranges. Figure 1 shows two of those ranges (left and middle) as illustration. The central peak at  $(\Delta\eta^*, \Delta\phi^*) = (0, 0)$ , present in both plots and truncated for better visualization, is the result of short-range correlations from the parton shower and hadronization. The far-side ridge at  $\Delta\phi^* \approx \pi$  is mostly related to back-to-back particle production and momentum conservation. Both these features have also been found in previous analyses of pp collisions, where they can also be reproduced using MC simulations. Similarly, for high- and inclusive  $N_{\text{ch}}^j$  classes in data, PYTHIA8 and SHERPA, strong away-side correlations are found, consistent with dominant contributions of back-to-back momentum conservation.

Another feature commonly observed in AA collisions is the ‘‘near-side ridge’’, an enhancement as seen in fig. 1 around  $\Delta\phi^* \approx 0$  over a long range in  $\Delta\eta^*$ . The  $N_{\text{ch}}^j$  reached in the single jet system shown in the middle plot is comparable to the event multiplicity of pp collisions, where a near-side ridge was first observed using a laboratory frame analysis [8]. The left plot corresponds to the case of inclusive jets (with  $\langle N_{\text{ch}}^j \rangle = 26$ ), where no suggestion of such a structure (around  $\Delta\phi \approx 0$ ) can be delineated, whereas

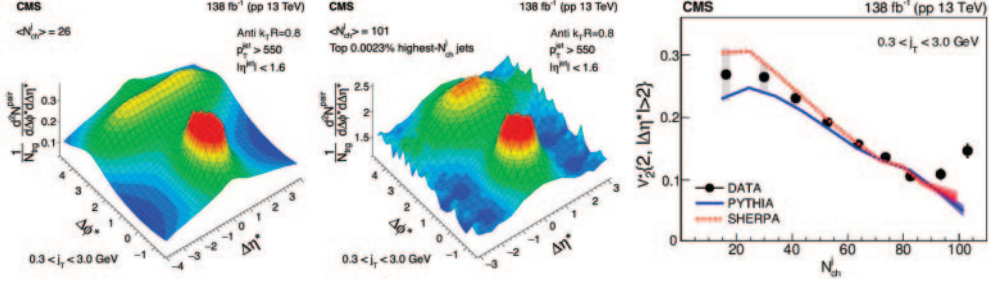


Fig. 1. – Results for 2D two-particle angular correlation in pp collisions at 13 TeV, considering anti- $k_T$   $R = 0.8$  jets with  $p_T^{\text{jet}} > 550$  GeV and  $|\eta| < 1.6$ , for  $0.3 < j_T < 3.0$  GeV, from all jet multiplicities (left) and for the highest in-jet  $N_{\text{ch}}^j$  (middle). The corresponding single-particle elliptic anisotropies  $v_2^*$ , as a function of  $N_{\text{ch}}^j$  (right), are also shown from data, PYTHIA8, and SHERPA. Vertical bars on data points indicate statistical uncertainties, shaded boxes represent systematic uncertainties. The shaded envelope around the MC curves show statistical uncertainty.

in the middle plot of fig. 1 some indication of a near-side ridge in the high- $N_{\text{ch}}^j$  (with  $\langle N_{\text{ch}}^j \rangle = 101$ ) can be seen, although this feature is less prominent than the ridges observed in pp and pA collisions. It is important to emphasize that no corresponding clear near-side enhancement is visible in the high- $N_{\text{ch}}^j$  2D distributions from either PYTHIA8 or SHERPA.

The 1D  $\Delta\phi^*$  correlation functions are extracted using eq. (2) and averaged over  $|\Delta\eta^*| > 2$  for particles with  $0.3 < j_T < 3.0$  GeV from jets in two  $N^j$  classes. The Fourier fits are used to extract the two-particle Fourier coefficient  $V_{2\Delta}^*$  and then the single-particle elliptic anisotropies  $v_2^* = \sqrt{V_{2\Delta}^*}$ , in the jet basis, as a function of  $N_{\text{ch}}^j$  inside the jet, for particles with  $0.3 < j_T < 3.0$  GeV. The result is shown in fig. 1 (right). Again, the MC simulation is generally successful at describing the data over a wide  $N_{\text{ch}}^j$  range. For jets at  $N_{\text{ch}}^j > 80$ , however, the value  $v_2^*$  no longer diminishes as  $1/N_{\text{ch}}^j$ , as would be expected if only short-range few-body correlation were present. Instead, the data start to show a steady increases with  $N_{\text{ch}}^j$ . Such an increase of  $v_2^*$  for very high- $N_{\text{ch}}^j$  jets is not observed in either PYTHIA8 or SHERPA and may be an indication of a possible onset of new QCD effects, *e.g.*, collectivity, in the parton fragmentation processes, for  $N_{\text{ch}}^j > 80$ . More details about this analysis and a complete discussion of the systematic uncertainties involved can be found in ref. [16].

## 2. – Measuring the speed of sound in PbPb collisions at LHC

The hot and dense medium formed in ultrarelativistic nuclear collision, QGP, exhibits collective dynamics and has macroscopic properties that are well described by nearly ideal relativistic hydrodynamics, for whose solution the initial conditions and the equation of state (EoS) are essential ingredients. In fluid-like environments, the study of sound modes arising from longitudinal compression waves provides a means to determine the corresponding speed of sound,  $c_s$ . This parameter, whose square is defined as the rate of change in pressure  $P$  in response to variations in energy density  $\varepsilon$ ,  $c_s^2 = dP/d\varepsilon$ [11], is decisive in characterizing the nature of the medium under investigation and in constraining the EoS.

In what follows, we discuss experimental results [25] for a new hydrodynamic probe [26] in lead-lead PbPb collisions with center-of-mass energy per nucleon pair of

$\sqrt{s_{\text{NN}}} = 5.02$  TeV, collected by the CMS experiment ref. [27] at the LHC. This novel technique uses the dependence of the mean transverse momentum  $\langle p_{\text{T}} \rangle$  on the charged particle multiplicity  $N_{\text{ch}}$  at a fixed  $\sqrt{s_{\text{NN}}}$  in collisions in which the ions almost entirely overlap (*i.e.*, at a very small impact parameter  $b$ ), known as “ultra-central” collisions. Recently, this correspondence was tested in [28] by running hydrodynamic simulations at zero impact parameter with several EoS and colliding energies, and was found to be precise.

As described in ref. [29], the speed of sound in the medium is predicted to be related to  $\langle p_{\text{T}} \rangle$  and  $N_{\text{ch}}$  as

$$(3) \quad c_s^2 = \frac{dP}{d\varepsilon} = \frac{s dT}{T ds} = \frac{d\langle p_{\text{T}} \rangle / \langle p_{\text{T}} \rangle}{dN_{\text{ch}} / N_{\text{ch}}},$$

where  $P$ ,  $\varepsilon$ ,  $s$  and  $T$  are the pressure, energy density, entropy density and temperature, respectively. To constrain the EoS, a simultaneous determination of  $c_s^2$  and its corresponding temperature is necessary. In terms of experimental observables,  $s$  is directly proportional to  $N_{\text{ch}}$ , while the temperature  $T$  is related to the average transverse momentum of emitted particles with respect to the beam axis  $\langle p_{\text{T}} \rangle$ . Hydrodynamic simulations in Refs. [26, 29] show that  $\langle p_{\text{T}} \rangle / 3$  is a good estimator of an effective temperature  $T_{\text{eff}}$  of the QGP phase. The  $T_{\text{eff}}$  can be interpreted as the initial temperature that a uniform fluid at rest would have, possessing the same amount of energy and entropy of the QGP fluid as it reaches its freeze-out state, when the quarks become bound into hadrons. Because of the longitudinal expansion and cooling of the system, the value of  $T_{\text{eff}}$  is generally lower than the initial temperature of the QGP fluid. Below,  $c_s^2$  is extracted for a specific  $T_{\text{eff}}$  and compared with theoretical models of relativistic nuclear collisions and predictions from lattice quantum chromodynamics (QCD).

The main experimental observable is the  $\langle p_{\text{T}} \rangle$  of charged particles in an event as a function of  $N_{\text{ch}}$ , where  $\langle p_{\text{T}} \rangle$  and  $N_{\text{ch}}$  are measured within the same pseudorapidity ( $|\eta| < 0.5$ ) and  $p_{\text{T}}$  ranges. Average  $p_{\text{T}}$  spectra for  $p_{\text{T}} > 0.3$  GeV are measured for events in 50 GeV intervals of the sum of the transverse energy  $E_{\text{T,sum}}^{\text{HF}}$  in the CMS forward hadron calorimeter (HF), from 3400 GeV to 5200 GeV, where tracking efficiency and misreconstruction effects are corrected. For avoiding any bias on estimating  $\langle p_{\text{T}} \rangle$  and  $N_{\text{ch}}$ , it is necessary to extrapolate the measured  $p_{\text{T}}$  spectra to  $p_{\text{T}} > 0$  GeV [26]. The resulting  $\langle p_{\text{T}} \rangle$  values from all  $E_{\text{T,sum}}^{\text{HF}}$  intervals are then plotted against the corresponding  $N_{\text{ch}}$  values to form the final observable.

The extraction of the speed of sound mainly depends on the relative variation of  $\langle p_{\text{T}} \rangle$  with respect to  $N_{\text{ch}}$  (see eq. (3)), therefore, normalized quantities,  $\langle p_{\text{T}} \rangle^{\text{norm}} = \langle p_{\text{T}} \rangle / \langle p_{\text{T}} \rangle^0$  and  $N_{\text{ch}}^{\text{norm}} = N_{\text{ch}} / N_{\text{ch}}^0$ , are used as the primary observables. Normalizing both  $\langle p_{\text{T}} \rangle$  and  $N_{\text{ch}}$  by their values in the reference event class can minimize most of the systematic uncertainties. The  $\langle p_{\text{T}} \rangle^0 = \langle p_{\text{T}} \rangle^{0-5\%}$  and  $N_{\text{ch}}^0 = N_{\text{ch}}^{0-5\%}$  represent the mean transverse momentum and charged multiplicity for the 0–5% centrality (*i.e.*, degree of overlap between the two Pb nuclei, with 0% representing their highest overlap). Here, the centrality class only needs to be close to that used for the  $c_s^2$  determination.

To extract the speed of sound, the expression that describes  $\langle p_{\text{T}} \rangle^{\text{norm}}$  as a function of  $N_{\text{ch}}^{\text{norm}}$  is taken from ref. [26], as

$$(4) \quad \langle p_{\text{T}} \rangle^{\text{norm}} = \left( \frac{N_{\text{ch}}^{\text{norm}}}{\mathcal{P}(N_{\text{ch}}^{\text{norm}})} \right)^{c_s^2},$$

where  $\mathcal{P}(N_{\text{ch}}^{\text{norm}})$  is a function used to correct for effects of charged particle multiplicity fluctuations for a fixed impact parameter; its parameters are extracted by fitting a charged particle multiplicity distribution in data [25]. After extracting the parameters of  $\mathcal{P}(N_{\text{ch}}^{\text{norm}})$ , a fit to the measured  $\langle p_{\text{T}} \rangle$  as a function of  $N_{\text{ch}}$  in data is performed by eq. (4) to extract  $c_s^2$ .

The measured multiplicity dependence of the  $\langle p_{\text{T}} \rangle$  is presented in fig. 2 (left), together with simulated results from Trajectum [30, 31] and from Gardim et al. [26, 29]. The measured  $\langle p_{\text{T}} \rangle^{\text{norm}}$  values first show a very soft decreasing trend toward a local minimum around  $N_{\text{ch}}^{\text{norm}} \sim 1.05$ . A rapid rise is observed at higher multiplicities, corresponding to ultra-central PbPb events. The observed trend, including the minimum around  $N_{\text{ch}}^{\text{norm}} \sim 1.05$ , is qualitatively described by the Trajectum model. Also, the model by Gardim et al. predicts a rise of  $\langle p_{\text{T}} \rangle^{\text{norm}}$  at very high multiplicities, with a slope similar to that observed in the data. However, it shows a flat trend at lower multiplicities, instead of the local minimum around  $N_{\text{ch}}^{\text{norm}} \sim 1.05$ .

To directly extract the speed of sound, the multiplicity dependence of the  $\langle p_{\text{T}} \rangle^{\text{norm}}$  data in fig. 2 (left) is fitted by eq. (4). Because the observed local minimum is not captured by the simplified model in eq. (4), the fit is performed only in the high-multiplicity range of  $N_{\text{ch}}^{\text{norm}} > 1.14$ , where the value of the goodness-of-fit is the best. The final result of the squared speed of sound,  $c_s^2$ , is found to be  $0.241 \pm 0.002$  (stat)  $\pm 0.016$  (syst) in natural units. The same fit is also performed to the prediction from the Trajectum model, resulting in  $c_s^2 = 0.283 \pm 0.045$ , where the model uncertainty is determined within the allowed parameter space constrained by a global Bayesian analysis [30, 31]. More recent studies [32] have shown that the slope of the steep rise of  $\langle p_{\text{T}} \rangle$  vs.  $N_{\text{ch}}$  can depend on the simulation parameters used to describe the initial transverse energy density and also on the centrality selection definition, in addition to the EoS. Regarding the former, it is important to note that correlations between these parameters and  $N_{\text{ch}}$  were not taken into account in ref. [32], which, if considered, could constrain the parameter values that influence the slope. Regarding centrality, studies using the CMS data recommend

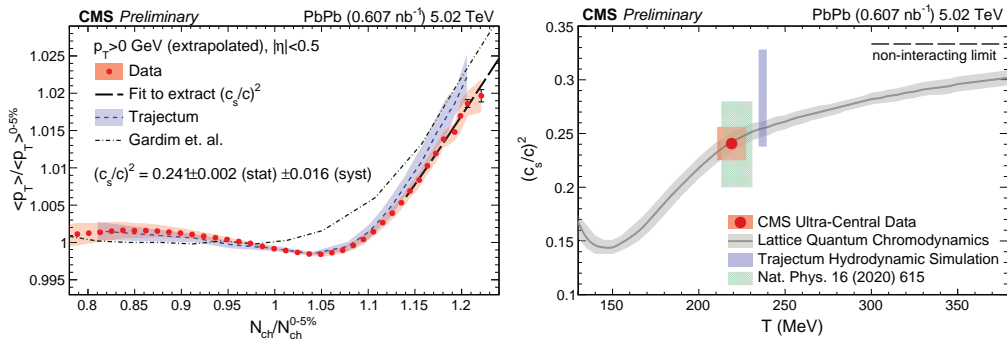


Fig. 2. – The average transverse momentum  $\langle p_{\text{T}} \rangle$  of charged particles is shown as a function of the charged particle multiplicity  $N_{\text{ch}}$  within the range  $|\eta| < 0.5$  and extrapolated to  $p_{\text{T}} > 0$  GeV (left). Both  $\langle p_{\text{T}} \rangle$  and  $N_{\text{ch}}$  are normalized by their values in the 0–5% centrality class. Bars and bands correspond to statistical and systematic uncertainties, respectively [25]. The speed of sound is shown as a function of the temperature (right). The size of the red box indicates systematic uncertainties of  $c_s^2$  and  $T$ . The values from Trajectum are extracted using the same procedure as in data. The curve shows the prediction from lattice QCD calculations. The dashed line at the value  $(c_s/c)^2 = 1/3$  corresponds to the upper limit for noninteracting, massless (“ideal”) gas systems [25].

to consider a large  $\eta$ -gap between the definition of centrality and the measured  $\langle p_T \rangle$  and  $N_{\text{ch}}$  for obtaining stable results, as done in the present analysis.

The  $T_{\text{eff}}$  is measured as  $T_{\text{eff}} = \langle p_T \rangle^0 / 3 = 219 \pm 8 (\text{syst})$  MeV, where the statistical uncertainty is negligible. Figure 2 (right) shows  $c_s^2$  as a function of  $T$ , with the CMS data point at  $T_{\text{eff}}$ . The results are compared with lattice QCD predictions [33], the Trajectum model, and the  $c_s^2$  value extracted in ref. [29]. The new CMS data allow for an remarkable degree of precision in the experimental determination of the speed of sound at this effective temperature. The results exhibit excellent agreement with the lattice QCD prediction, with comparable uncertainties. Thus, these findings provide compelling and direct evidence for the formation of a deconfined QCD phase at LHC energies. This relatively simple procedure can be applied to different colliding systems and energies. If systematically compared with calculations from lattice QCD, it can be used to help the search for the QCD phase transition and the critical point. Is important to note that first attempts to extract the speed of sound in ultrarelativistic collisions at lower center of mass energies were performed by analyzing rapidity distributions [34, 35], extracting values for  $c_s^2$  of similar order as in the present work.

### 3. – Summary

The initial part of this contribution discusses the first search for long-range near-side correlations and quantum chromodynamics (QCD) collective effects in jets produced in proton-proton collisions at  $\sqrt{s} = 13$  TeV. The measurement is performed using charged constituents from individual jets, after calculating their kinematic variables in a coordinate system where the  $z$ -axis coincides with the jet direction. Two-particle correlations are studied as a function of the number of charged constituents in the jet,  $N_{\text{ch}}^j$ . The second Fourier harmonics of long-range azimuthal correlations are extracted and compared with those calculated with PYTHIA8 and SHERPA Monte Carlo (MC) event generators, used to model the parton fragmentation process. While the data and MC predictions are in good agreement for low- and mid- $N_{\text{ch}}^j$  particle correlations inside jets, the extracted single-particle long-range elliptic azimuthal anisotropy  $v_2^*$  shows a distinct increase in data for  $N_{\text{ch}}^j > 80$ . Such result suggests a possible onset of collective behavior in the high-multiplicity range, which is not reproduced by the MC simulations.

The second half of these contribution presents a measurement of a new hydrodynamic probe that results in the most precise extraction to date of the squared speed of sound of  $0.241 \pm 0.002 (\text{stat}) \pm 0.016 (\text{syst})$  (in natural units) in ultrarelativistic nuclear collisions at an effective temperature of  $219 \pm 8 (\text{syst})$  MeV. The measurement is performed by determining the dependence of the mean transverse momentum on the total charged particle multiplicity in nearly head-on lead-lead collisions with center-of-mass energy per nucleon pair of  $\sqrt{s_{\text{NN}}} = 5.02$  TeV. The excellent agreement of lattice QCD predictions with the experimental results provides strong evidence for the existence of a deconfined phase of quantum chromodynamics matter at extremely high temperatures and small chemical potential. This method applied to other colliding systems and energies can contribute to the search for the phase transition and the critical point in high-density QCD.

\* \* \*

This contribution is based on work partially supported by FAPESP (Proc. N. 2018/25225-9) and CNPq (Proc N. 312369/2019-0).

## REFERENCES

- [1] STAR COLLABORATION, *Nucl. Phys. A*, **757** (2005) 102.
- [2] PHENIX COLLABORATION, *Nucl. Phys. A*, **757** (2005) 184.
- [3] BRAHMS COLLABORATION, *Nucl. Phys. A*, **757** (2005) 1.
- [4] PHOBOS COLLABORATION, *Nucl. Phys. A*, **757** (2005) 28.
- [5] STAR COLLABORATION (ADAMS J. *et al.*), *Phys. Rev. Lett.*, **95** (2005) 152301.
- [6] ALICE COLLABORATION (AAMODT K. *et al.*), *Phys. Rev. Lett.*, **105** (2010) 252302.
- [7] CMS COLLABORATION (CHATRCHYAN S. *et al.*), *Phys. Lett. B*, **718** (2013) 795.
- [8] CMS COLLABORATION (KHACHATRYAN V. *et al.*), *JHEP*, **09** (2010) 091.
- [9] BADEA A. *et al.*, *PoS*, **ICHEP2018** (2019) 446.
- [10] BELLE COLLABORATION (CHEN Y.-C. *et al.*), *Phys. Rev. Lett.*, **128** (2022) 142005.
- [11] ZEUS COLLABORATION (ABT I. *et al.*), *JHEP*, **04** (2020) 070.
- [12] ZEUS COLLABORATION (ABT I. *et al.*), *JHEP*, **12** (2021) 102.
- [13] CMS COLLABORATION (TUMASYAN A. *et al.*), *Phys. Lett. B*, **844** (2023) 137905.
- [14] ATLAS COLLABORATION (AAD G. *et al.*), *Phys. Rev. C*, **104** (2021) 014903.
- [15] BATY A., GARDNER P. and LI WEI, *Phys. Rev. C*, **107** (2023) 064908.
- [16] CMS COLLABORATION, *CMS Physics Analysis Summary HIN-21-013* (2023), <https://cds.cern.ch/record/2884812>.
- [17] BERTOLINI D. *et al.*, *JHEP*, **10** (2014) 059.
- [18] CACCIARI M., SALAM G. P. and SOYEZ G., *JHEP*, **04** (2008) 063.
- [19] CACCIARI M., SALAM G. P. and SOYEZ G., *Eur. Phys. J. C*, **72** (2012) 1896.
- [20] SJOSTRAND T., MRENNNA S. and SKANDS P. Z., *Comput. Phys. Commun.*, **178** (2008) 852.
- [21] CMS COLLABORATION (SIRUNYAN A. M. *et al.*), *Eur. Phys. J. C*, **80** (2020) 4.
- [22] BOTHMANN E. *et al.*, *SciPost Phys.*, **7** (2019) 034.
- [23] CMS COLLABORATION, *CMS Physics Analysis Summary, HIN-23-003* (2023), <https://cds.cern.ch/record/2886388>.
- [24] HEINZ U. and SNELLINGS R., *Annu. Rev. Nucl. Part. Sci.*, **63** (2013) 123.
- [25] CMS COLLABORATION, *CMS Physics Analysis Summary, HIN-23-003* (2023), <https://cds.cern.ch/record/2870141>.
- [26] GARDIM F. G., GIACALONE G. and OLLITRAULT, J. -Y. , *Phys. Lett. B*, **809** (2020) 135749.
- [27] CMS COLLABORATION, *JINST*, **3** (2008) S08004.
- [28] GARDIM F. G., GIANNINI A. V. and OLLITRAULT J.-Y., arXiv:2403.06052 (2024).
- [29] GARDIM F. G., GIACALONE G., LUZUM, M. and OLLITRAULT J. -Y., *Nat. Phys.*, **16** (2020) 615.
- [30] NIJS G. and VAN DER SCHEE W., *Phys. Rev. C* , **106** (2022) 044903.
- [31] GIACALONE G., NIJS, G. and VAN DER SCHEE W., arXiv:2305.00015 (2023), to be published.
- [32] NIJS G. and VAN DER SCHEE W., arXiv:2312.04623 (2023), to be published.
- [33] HOTQCD COLLABORATION, *Phys. Rev. D*, **90** (2014) 094503.
- [34] MOHANTY B. and ALAM J., *Phys. Rev. C*, **68** (2003) 064903.
- [35] NA57 COLLABORATION, *J. Phys. G: Nucl. Part. Phys.*, **31** (2005) 1345.
- [36] CHEN Y.-C. *et al.*, arXiv:2312.05084 (2023), to be published.